Preparation and Characterization of Polysulfone/Sulfonated Polysulfone/Cellulose Nanofibers Ternary Blend Membranes

Lili Zhong, Zhaodong Ding, Bei Li, and Liping Zhang *

Ternary blend membranes were prepared with polysulfone (PSf), sulfonated polysulfone (SPSf), and cellulose nanofibers (CNF) by a Loeb-Sourirajan (L-S) phase inversion process. The cross-section and bottom surface morphology of the membranes were analyzed by scanning electron microscopy (SEM), and the performance of the membranes was evaluated in terms of pure water flux, bovine serum albumin (BSA) rejection, contact angle, tensile strength, and breaking elongation. The morphology of the cellulose nanofibers (CNF) was detected by transmission electron microscopy (TEM). Results showed that within a certain range, the addition of SPSf improved compatibility between PSf and CNF, and the addition of CNF could improve the hydrophilicity of the membranes. The maximum value of pure water flux reached 137.6 L/m^{2}h, and the minimum value of BSA rejection reached 95.8% when CNF content was 0.3 wt% in casting solution. Also, a certain addition of CNF could enhance the mechanical properties of the membranes.

Contact information: Beijing Key Laboratory of Lignocellulosic Chemistry, Beijing Forestry University, No.35 Tsinghua East Road, Haidian District, Beijing, 100083, PR China;
* Corresponding author: zhanglp418@163.com

INTRODUCTION

In the past several years, synthetic polymeric membranes have been used for a wide variety of liquid separations. The Loeb-Sourirajan (L-S) phase-inversion process is a common method for the preparation of asymmetrical polymeric membranes (Rahimpour *et al.* 2010). L-S phase-inversion process involves conversion of a homogeneous polymer solution consisting of two or more components to a two-phase system, the solid polymer rich phase and the liquid polymer poor phase. The solid phase forms the membrane structure, while the liquid phase forms the membrane pores (Ma *et al.* 2011). Polysulfone (PSf) is widely used as a membrane material because of its excellent properties, including the ability to form chemically stable membranes easily with excellent heat-resistant properties (Abu-Thabit *et al.* 2012; Tran *et al.* 2012; Gong *et al.* 2013). PSf membranes are also widely applied in contemporary water treatment, hemodialysis, and desalination processes (Chang *et al.* 2010; Jutemar and Jannasch 2010; Padaki *et al.* 2012; Kumar *et al.* 2013a; Kumar *et al.* 2013b). However, the use of polysulfone for the aqueous phase is limited by its intrinsic hydrophobicity. It is generally accepted that increasing hydrophilicity can improve the antifouling property of membranes (Rahimpour *et al.* 2007; Zhao *et al.* 2014). Blending may also be a suitable modification for improving the hydrophilicity of polysulfone membranes. Blending different polymers conserves their individual superior properties in the final mixture while concurrently reducing their poor

characteristics. It is an extremely attractive and inexpensive way of obtaining new structural materials. This has stimulated great interest in the preparation of membranes for improving their properties and morphological structures (Arthanareeswaran *et al.* 2008). However, the choice of polymers depends upon both the compatibility of the individual polymers with each other and the homogenous blending method (Arthanareeswaran *et al.* 2007).

Cellulose is the most abundant natural biopolymer found in the world, and it has considerable advantages, such as environmental friendliness, biodegradability, and renewability (Goetz *et al.* 2009; Li *et al.* 2009; Zuluaga *et al.* 2009). Many different kinds of cellulose materials exist in nano-scale. The acid based and the mechanical processed materials are different. Sulfuric acid hydrolysis of cellulose is a well-known process used to remove amorphous regions (Rosa *et al.* 2010), and high-pressure homogenization can provide cellulose with smaller dimensions and a larger surface area. After these chemical and mechanical processes, cellulose nanofibers (CNF) were obtained. CNF has abundant hydroxyl groups, small dimensions, and has greater specific surface area compared with larger size materials. This provides CNF with high hydrophilicity and high mechanical properties, which makes it an effective reinforcing filler for various composite materials. According to previous literature reports, various cellulose nanoparticles have been composited with polysulfone or polyether sulfone to enhance the hydrophilicity and mechanical properties of the membrane (Qu *et al.* 2010; Li *et al.* 2011). In order to further improve the hydrophilicity and mechanical properties of the membranes, it is necessary to improve the intermolecular compatibility between PSf and CNF.

Sulfonated polysulfone (SPSf) is produced by the sulfonation of polysulfone; therefore its molecular structure is similar to polysulfone. SPSf has film-forming capacity, good flexibility, and high chemical and thermal stabilities (Xin and Wang 1994; Chen *et al.* 2001; Geise *et al.* 2010). It also has exceptional mechanical properties, as well as excellent chemical and electrochemical stability related to the presence of the rigid backbone (Deimede *et al.* 2014). The intermolecular compatibility between PSf and SPSf is high with a certain proportion of composition. Because SPSf has hydroxyl groups in its molecular structure, intermolecular hydrogen bonds can be generated between the hydroxyl groups of cellulose and SPSf. Thus, the intermolecular compatibility between PSf and CNF can be promoted through SPSf.

In the present work, PSf/SPSf/CNF ternary blend membranes were prepared by the L-S phase inversion process. The blend membranes were characterized by Fourier transform infrared spectroscopy (FTIR) and analysis of the structure. Variations in the morphology of the blend membranes were analyzed by scanning electron microscopy (SEM). The effects of different CNF content on pure water flux, BSA rejection, contact angle, porosity, as well as the mechanical properties of the blend membranes were investigated in detail. The dimensions and morphology of CNF were detected by transmission electron microscopy (TEM).

EXPERIMENTAL

Materials

Lignocellulose pulp board was purchased from Shandong Huatai Paper Co., Ltd. (Shandong Province, China). Polysulfone (PSf, η=0.58) was purchased from Dalian polysulfone Plastics Co., Ltd. (Liaoning Province, China). Sulfonated polysulfone (SPSf,

degree of sulfonation=0.1) was purchased from Shanghai Chunyi New Material Technology Co., Ltd. (Shanghai, China). Sulfuric acid (H_2SO_4, 98 wt.%) and N, N-dimethylacetamide (DMAc) were purchased from the Beijing Chemical Plant (Beijing, China). Polyethylene glycol (PEG) (molecular weight 400, AR) was purchased from Sinopharm Chemical Reagent Co., Ltd. (Shanghai, China). Tungstophosphoric acid was purchased from Tianjin Jinke Fine Chemical Research Institute (Tianjin, China). Bovine serum albumin (BSA) was purchased from Beijing Aoboxing Biological Technology Co., Ltd. (Beijing, China).

Preparation of Cellulose Nanofibers (CNF) in DMAc

Lignocellulose pulp board was added to 15 wt.% sulfuric acid at 85 °C for 4 h under mechanical stirring with a speed of 500 rpm, and the solid to liquid ratio was 1:40. The suspension was washed with deionized water and concentrated by centrifugation. Then it was subjected to dialysis against water until it reached neutrality. The neutral suspension was then vacuum filtered, and the solids were washed with DMAc to remove the water. After that, the solids were immersed into DMAc and homogenized with a homogenizer (NS1001S2K, GEA NiroSoavi Co., Italy) at a high pressure of 100 MPa. Through this process, the CNF was well-dispersed into the DMAc.

Membrane Preparation

The well-dispersed CNF suspension was diluted into different concentrations as follows: 0.1 wt.%, 0.2 wt.%, 0.3 wt.%, 0.4 wt.%, and 0.5 wt.%. The predetermined amounts of PSf and SPSf were dissolved in the prepared CNF suspension, and the total concentration of PSf and SPSf was 18 wt.%. Also, 5 wt.% PEG 400 was added to the aforementioned solution. The solution was mechanically stirred at 50 °C for at least 8 h to guarantee complete dissolution of the polymer. The casting solution was left still for 24 h to allow the complete release of bubbles (Zhao *et al*. 2011). The membranes were prepared through an immersed phase-inversion process. A small amount of each casting solution (Table 1) was poured onto an undefiled glass plate, then scraped by a home-made scraper. Any DMAc present in the casting solutions was allowed to evaporate for 30 s; then it was immediately immersed into a coagulating bath of deionized water. The membrane was washed with deionized water to remove the residual solvent and porogen, then stored in deionized water for at least 24 h before testing.

Table 1. Composition of Casting Solutions

Membranes	PSf(wt.%)	SPSf(wt.%)	CNF(wt.%)	PEG 400(wt.%)	DMAc(wt.%)
M1	18.0	-	-	5	77.0
M2	17.1	0.9	-	5	77.0
M3	16.2	1.8	-	5	77.0
M4	15.3	2.7	-	5	77.0
M5	14.4	3.6	-	5	77.0
M6	16.2	1.8	0.1	5	76.9
M7	16.2	1.8	0.2	5	76.8
M8	16.2	1.8	0.3	5	76.7
M9	16.2	1.8	0.4	5	76.6
M10	16.2	1.8	0.5	5	76.5

Characterization

Transmission electron microscopy (TEM)

Transmission electron microscopy (TEM, JEM-1010, JEOL, Japan) was used to determine the dimensions of the CNF with an accelerating voltage of 80 kV. To enhance contrast in TEM, the CNF were negatively stained with a 2 wt.% aqueous solution of phosphotungstic acid for 1 min.

Fourier transform infrared spectroscopy (FTIR)

The chemical structure characterizations of the membranes were tested with a Fourier transform infrared spectrometer (FTIR, VERTEX 70V, Bruker, Germany) with the attenuated total reflectance (ATR, PIKE, USA) accessory. The measured wavenumber range was 4000 to 600 cm^{-1}.

Differential scanning calorimetry (DSC) analysis

The Differential scanning calorimetry (DSC) analysis was determined with materials weight of about 2.0 to 3.0 mg, and started heating from 50 °C to 250 °C at the rate of 10 °C /min.

Scanning electron microscopy (SEM)

The cross-section and bottom surface morphologies of the membranes were observed using scanning electron microscopy (SEM, S-3400n, Hitachi, Japan) with an accelerating voltage of 5 kV and a scanning electron microscope with an accelerating voltage of 3 kV (FE-SEM, SU8000, Hitachi, Japan).

Flux and retention

Pure water flux was measured by a self-made ultrafilter. The initial water flux was taken about 30 min after pressurization in the ultrafilter, at 0.15 MPa, and working at 0.1 MPa during the test. Pure water flux (J_w) was calculated using the following equation (Eq. 1),

$$J_w = \frac{Q}{(A \times \Delta t)},$$ (1)

where Q is the permeation of pure water (L), A is the effective membrane area (m^2), and Δt (h) is the sampling time.

The BSA rejection (R) of membranes was measured by calculating the fluid retention capacity of BSA through the membranes using a UV-spectrophotometer (UV-1801, BFRL, China) to measure the absorbance of the BSA solution (1 g/L) and the permeation solution at 280 nm. All tests were conducted at a working pressure of 0.1 MPa and at room temperature. The retention coefficient (R) was calculated as follows (Eq. 2),

$$R = \left(1 - \frac{A_1}{A_2}\right) \times 100\%,$$ (2)

where A_1 and A_2 are the absorbance of the filtrated and raw solutions of BSA, respectively.

Contact angle

The hydrophilicity of the membranes was examined using a water contact angle measuring instrument (JGW-360a, HAKE, China). Deionized water droplets were placed on the surface of the membranes, and then the contact angle was measured until no change was observed.

Mechanical tests

Tensile strength, breaking elongation, and tensile modulus were characterized by a computer-controlled tensile testing instrument (ZB-WL300, Hangzhou Zhibang Automated Instrument Co., Ltd., China). The stretching rate was 10 mm/min. To minimize the experimental error, the reported values were the average of five samples.

RESULTS AND DISCUSSION

Morphology of CNF

In this study, the methods of dilute sulfuric acid hydrolysis and physical high-pressure homogenization were used to prepare CNF suspensions. Figure 1 shows TEM images of the CNF derived from lignocellulose pulp board; the nanofibers were relatively uniformly dispersed in the DMAc. The length and width of the CNF were measured from the TEM images. The CNF had lengths ranging from 500 to 700 nm, and widths ranging from 20 to 40 nm. The CNF derived through the methods of dilute sulfuric acid hydrolysis and physical high-pressure homogenization indicated a range of aspect ratio from 15 to 20. According to their relatively high aspect ratios, the prepared CNF could be an effective reinforcement in nanocomposites for improving their mechanical properties (Rosa *et al.* 2010; Ang-atikarnkul *et al.* 2014).
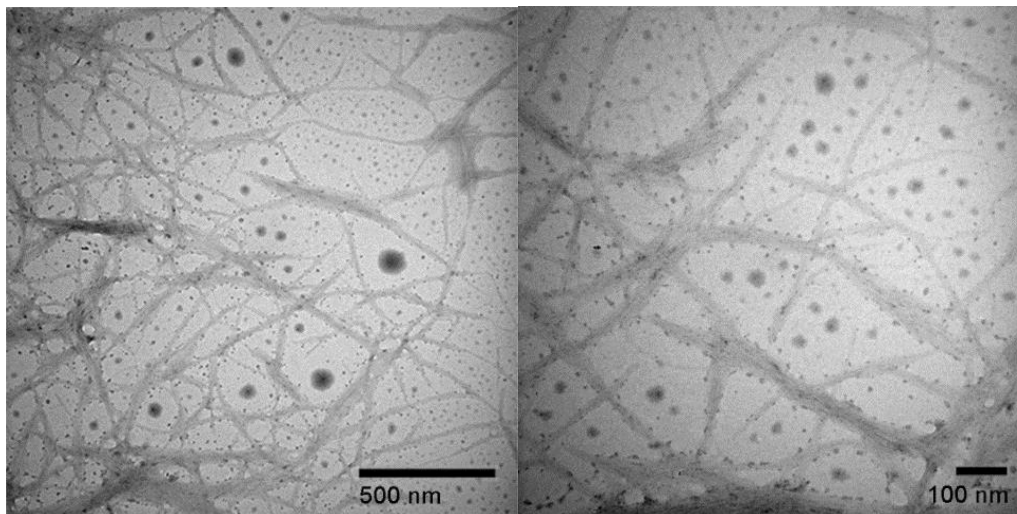

Fig. 1. Transmission electron microscope images of cellulose nanofibers

Fourier Transform Infrared Spectroscopy Analysis

Figure 2 shows the FTIR spectra of sample M1 (a), sample M3 (b), and sample M8 (c). Figure 2a is a typical FTIR spectra of PSf. The characteristic absorption peaks of the benzene ring were at 1585 cm^{-1} and 1488 cm^{-1}. The asymmetric absorption peaks of S=O

were at 1323 cm^{-1} and 1294 cm^{-1}, and the symmetric absorption peaks of S=O were at 1160 cm^{-1}. Compared with pure PSf membrane, the addition of sulfonated polysulfone caused the membrane to have a wide absorption peak at 3525 cm^{-1}, which is the characteristic absorption peak of hydroxyl that was derived from the sulfonic acid group. Hydroxyl groups can improve the hydrophilicity of the membrane. Comparing spectra (b) with spectra (c), it can be observed that after blending CNF with the PSf/SPSf membrane, the hydroxyl characteristic absorption peak became wider and the peak value increased; thus the hydrophilicity of the membrane was further promoted. Also, the absorption peak moved to 3496 cm^{-1}, and compared with spectra (b), the absorption peak moved to a low-frequency direction for 29 cm^{-1}. It can be shown that intermolecular hydrogen bonds were generated between the hydroxyl groups of CNF and the hydroxyl groups of SPSf, which means that the compatibility between PSf and CNF was promoted with the addition of SPSf.
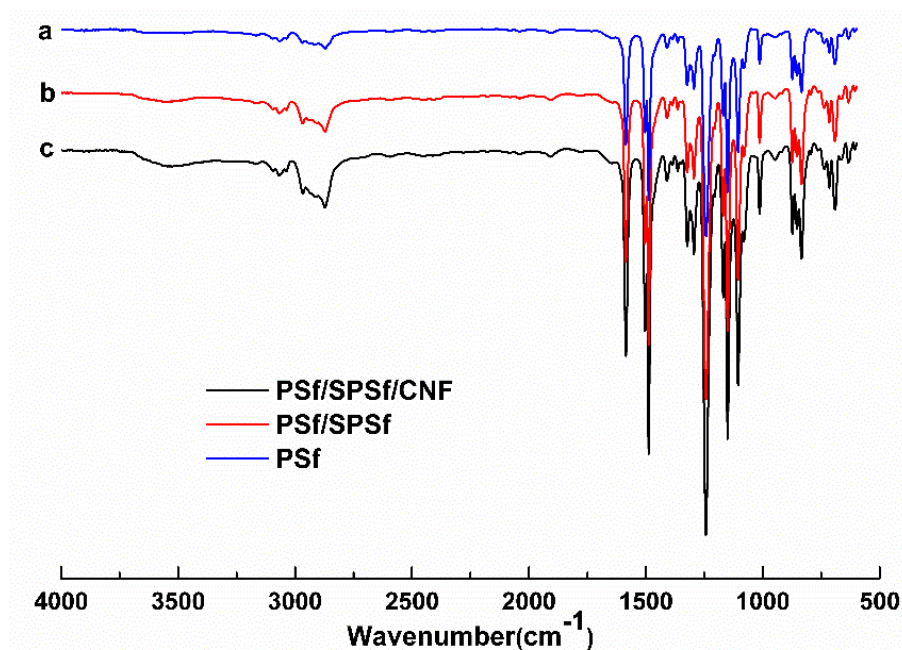
Fig. 2. FTIR spectra of pure PSf membrane (a), PSf/SPSf blend membrane (b), and PSf/SPSf/CNF blend membrane (c)

Compatibility of PSf/SPSf Casting Solutions

The DSC spectra of pure PSf membrane (a), PSf/SPSf blend membrane (b), and SPSf (c) are shown in Fig. 3. It could be observed that the spectra (a) had a wide range of glass transition temperature (T_g), approximately from 153 to 188 °C, and the spectra (c) showed that a characteristic glass transition temperature (T_g) of SPSf was exhibited at approximately 200 °C. The spectra (b) exhibited two compound peak approximately at 172 and 180 °C, and the T_g of PSf/SPSf blend membrane were closer than the T_g of pure PSf and SPSf, and all the T_g values stayed within the range from 153 to 200 °C. These results demonstrated that the PSf and SPSf were partially compatible, and the PSf/SPSf was a partially compatible system.

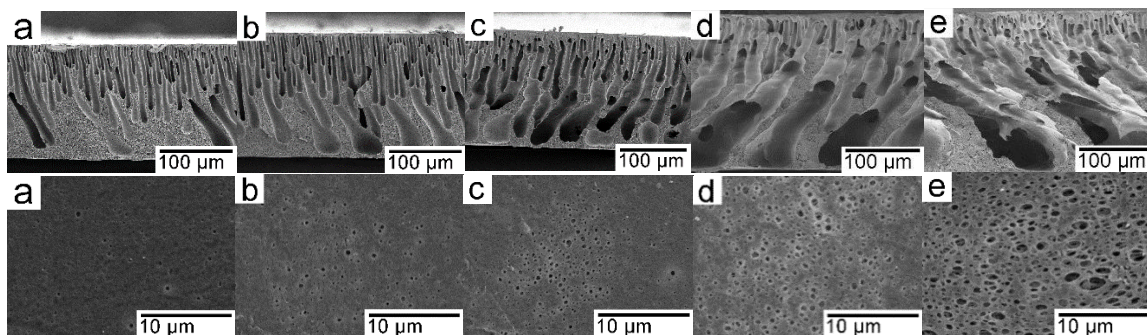## Morphological Study of the Membrane

As shown in Fig. 4, the cross-section and bottom surface morphology of pure PSf membrane, PSf/SPSf blend membrane, and PSf/SPSf/CNF blend membranes were

observed by SEM at 400× magnification for the overall cross-section and 5,000× magnification for the bottom surface.
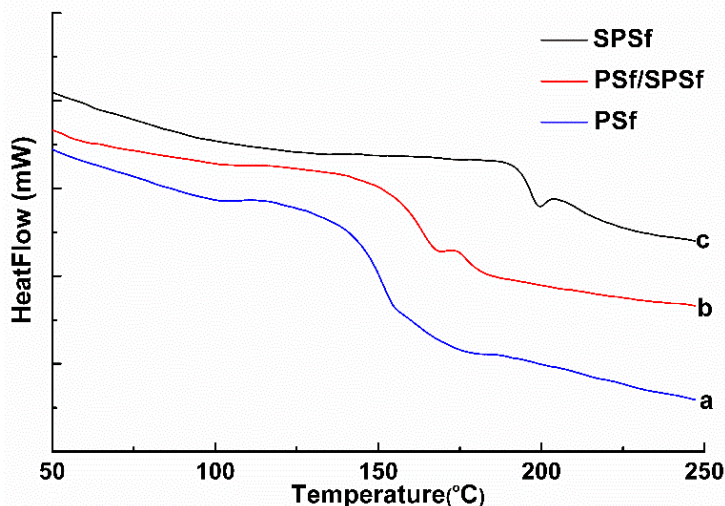
Fig. 3. DSC spectra of pure PSf membrane (a), PSf/SPSf blend membrane (b), and SPSf (c)

The pure PSf membrane exhibited the typical asymmetrical structure, which had thin and short finger-like pores. Comparing image (b) with image (a), it can be observed that the pore size and quantity in the bottom surface of the membrane were all increased with the addition of SPSf. Also, the connectivity of the finger-like pores were higher than that of pure PSf membrane. After the addition of CNF, the pore size and quantity in the bottom surface of the membrane were further increased. The cross-section seems to have finger-like pores the top surface and large voids near the bottom surface (Ma *et al*. 2011). The connectivity of the finger-like pores were better than the PSf/SPSf blend membrane, and there were some developed large voids in the cross-section of the PSf/SPSf/CNF blend membranes. With increasing CNF content in the blend membrane, the pore size and quantity of the bottom surface were increased, also the size of the finger-like pores in the cross-section increased and large voids were formed. However, when adding excess CNF into the blend membrane, the finger-like pores in the cross-section were shaped irregularly, and pore defects on the bottom surface of the membrane were formed (Fig. 4e).


Fig. 4. Cross-section and bottom surface SEM images of membranes: (a) M1, (b) M3, (c) M6, (d) M8, and (e) M10

This change in the morphologies could be attributed to the addition of SPSf and CNF, which increased the hydrophilicity of the membranes. These conditions accelerated the phase inversion process and also accelerated the growth of new phase nucleus formation in the polymer-poor phase. This also increased the interactions among components in the casting solution and phase inversion kinetics. Furthermore, the viscosity of the casting solutions were also increased by increasing the CNF content (Li *et al*. 2011). The CNF presented large aspect ratios and were therefore easily aggregated, which resulted in the pores of the blend membranes being easily blocked, as well as the formation of pore defects (Qu *et al*. 2010; Bai *et al*. 2015).

Pure Water Flux and BSA Rejection

The influence of the PSf/SPSf blend polymer composition on pure water permeability and BSA rejection are shown in Fig. 5a. The pure water flux of membranes increased from 44.1 L/m^{2}h to 103.6 L/m^{2}h with changes in PSf/SPSf composition in the casting solution from 100/0 to 80/20, and the BSA rejection of blend membranes decreased, but all remained above 97%. With increasing proportions of SPSf, the pure water flux of PSf/SPSf blend membranes was increased. However, it can also be clearly observed that the increase of pure water flux gradually slowed down when the proportion of PSf/SPSf composition was greater than 90/10. It had already been shown that the PSf and SPSf blending system in the experiment was a partial compatible system (Fig. 3). The increase in pure water flux gradually slowed down, which demonstrates that too much SPSf did not improve the hydrophilicity of the PSf membrane. Therefore, from what has been discussed above, the PSf/SPSf blend polymer composition of 90/10 was judged to be suitable for further experiments.
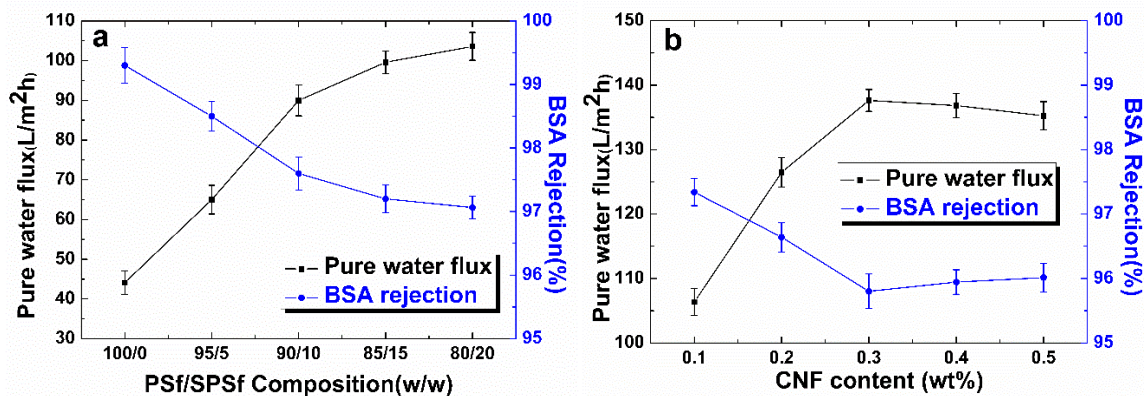
Fig. 5. (a) Effect of PSf/SPSf composition on pure water flux and BSA rejection of blend membranes; (b) effect of different CNF contents on pure water flux and BSA rejection of blend membranes

Figure 5b shows the pure water flux and BSA rejection of blend membranes with different CNF contents corresponding with samples of M6, M7, M8, M9, and M10, respectively. The pure water flux of blend membranes with increasing CNF content first increased, then decreased. The maximum value of pure water flux reached 137.6 L/m^{2}h when the CNF content was 0.3 wt.% in casting solution. The BSA rejection of blend membranes with increasing CNF content first decreased, then increased. Also, the minimum value of BSA rejection reached 95.8% when the CNF content was 0.3 wt.% in casting solution. The CNF itself contained a high ratio of exposed hydroxyl groups relative

to its tiny dimensions and large surface area, so CNF had a high moisture absorption capacity in order to facilitate the diffusion of water into the casting solution, and could therefore trigger the instantaneous phase separation process. With increasing CNF content in the casting solutions, the velocity of this process was increased. Thus, the interconnected finger-like pores formed more easily, and the quantity and size of the bottom surface pores were all increased, as can be observed from the SEM images. These factors all caused the significant increase of pure water flux, and also caused a decrease in BSA rejection. However, the addition of CNF could increase the viscosity of the casting solutions, and the CNF presented large aspect ratios and were therefore easily aggregated (Li *et al*. 2011). The worsening dispersion performance of CNF in the casting solution caused the compatibility between SPSf and CNF to decrease, and the weakening of intermolecular hydrogen bonding interactions also indirectly caused the compatibility between PSf and CNF to decrease. Also, adding too much CNF to the blend membranes could block membrane pores (Bai *et al*. 2015). These phenomena resulted in the slight decrease of pure water flux and the slight increase of BSA rejections when the addition of CNF content was more than 0.3 wt.%. These results demonstrated that 0.3 wt.% was a suitable amount of CNF addition to blend membranes.

Hydrophilicity of the Membrane

As shown in Table 2, the contact angle of the PSf/SPSf blend membrane was lower than that of the pure PSf membrane, indicating that the addition of SPSf enhanced the hydrophilicity of the membrane. This might be attributed to the hydroxyl groups of SPSf being close to membrane surface. Also, the contact angle of PSf/SPSf/CNF blend membranes were lower than that of PSf/SPSf blend membranes, indicating that the addition of CNF further enhanced the hydrophilicity of the membrane. This is likely because of the large surface area and abundant hydroxyl groups of CNF, and the finger-like pores became longer and large voids became wider with the increase of CNF content, which is good for its connectivity and results in the improvement of the membrane permeability (Bai *et al*. 2015). At the same time, with increasing CNF content in the membrane, the contact angle of PSf/SPSf/CNF blend membranes gradually decreased, but CNF clearly stopped enhancing the hydrophilicity of the membrane when its content in the membrane reached above a certain range. This might be attributed to excess CNF's inability to evenly disperse into the casting solution, resulting in decreased compatibility between PSf, SPSf, and CNF. The excess CNF might also have been washed away from the membrane during the phase inversion process.

Table 2. Contact Angle (CA) of the Membranes

Membrane	M1	M3	M6	M7	M8	M9	M10
CA (°)	74.7 ± 1.3	70.9 ± 1.7	66.3 ± 1.2	63.2 ± 1.8	61 ± 2.1	60.1 ± 1.7	59.5 ± 0.9

Mechanical Properties of the Membrane

The mechanical properties of the membranes are shown in Fig. 6. With the increase of CNF content in the blend membrane, the tensile strength, breaking elongation, and tensile modulus first increased, then decreased. The maximum values of the tensile strength, breaking elongation and tensile modulus reached 4.1MPa, 10.4%, and 181.6Mpa respectively, when the CNF content was 0.3 wt.% in casting solution. These results demonstrate that an appropriate amount of CNF could enhance the mechanical properties

of the blend membrane. Because of CNF's large surface area and abundant hydroxyl groups, cross-link network hydrogen bonds and interactions can be formed between the CNF and SPSf, and interfacial compatibility was enhanced by these hydrogen bonds. Also, the interfacial compatibility between PSf, SPSf, and CNF was enhanced in this way. This can also be evidenced by the improvement of the blend membrane's mechanical properties. However, the excess CNF was easy to aggregate and could not be evenly dispersed in the casting solution, resulting in decreased compatibility between PSf, SPSf, and CNF; pore defects; and the formation of large voids, which led to decreased tensile strength, breaking elongation and tensile modulus. (Qu *et al.* 2010; Li *et al.* 2011; Tang *et al.* 2014). Also, the excess CNF might have been washed away from the membrane during the phase inversion process. Therefore, too much addition of CNF could not enhance the mechanical properties of membranes.
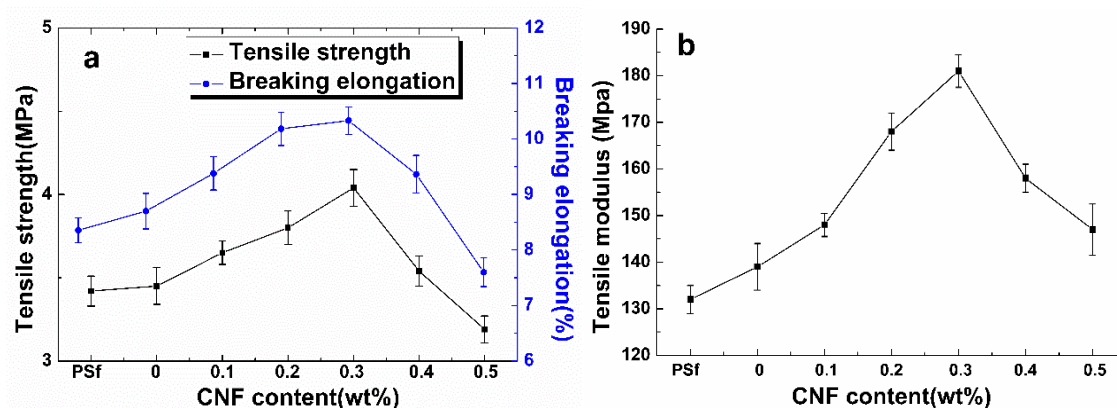
Fig. 6. (a) Tensile strength and breaking elongation of the membranes (M1, M3, M6, M7, M8, M9, and M10); (b) tensile modulus of the membranes (M1, M3, M6, M7, M8, M9, and M10)

CONCLUSIONS

1. PSf/SPSf/CNF ternary blend membrane was successfully prepared by the L-S phase inversion process. The morphology of CNF were measured from TEM images. FTIR analysis showed that intermolecular hydrogen bonds were generated between the hydroxyl groups of CNF and SPSf.

2. The compatibility of the PSf and SPSf blending system was evaluated, and the optimum proportion was chosen. The compatibility between PSf and CNF was promoted by adding SPSf.

3. The pore size and quantity of the bottom surface were increased after the addition of appropriate amounts of CNF, and the connectivity of finger-like pores were higher than that of the PSf membrane. The addition of CNF changed the structure of the membrane.

4. The maximum value of pure water flux reached 137.6 L/m^{2}h, and the minimum value of BSA rejection reached 95.8% when the CNF content was 0.3 wt.% in casting solution. The changes in contact angle demonstrated that the hydrophilicity of the membrane was increased with increasing CNF content in the membrane. Also, the addition of a certain amount of CNF can enhance the mechanical properties of the membranes.

ACKNOWLEDGMENTS

REFERENCES CITED

Abu-Thabit, N. Y., Ali, S. A., Zaidi, S. M. J., and Mezghani, K. (2012). "Novel sulfonated poly (ether ether ketone)/phosphonated polysulfone polymer blends for proton conducting membranes," *J. Mater. Res.* 27(15), 1958-1968. DOI: 10.1557/jmr.2012.145

Ang-atikarnkul, P., Watthanaphanit, A., and Rujiravanit, R. (2014). "Fabrication of cellulose nanofiber/chitin whisker/silk sericin bionanocomposite sponges and characterizations of their physical and biological properties," *Compos. Sci. Technol.* 96, 88-96. DOI: 10.1016/j.compscitech.2014.03.006

Arthanareeswaran, G., Mohan, D., and Raajenthiren, M. (2007). "Preparation and performance of polysulfone-sulfonated poly (ether ether ketone) blend ultrafiltration membranes. Part I," *Appl. Surf. Sci.* 253(21), 8705-8712. DOI: 10.1016/j.apsusc.2007.04.053

Arthanareeswaran, G., Thanikaivelan, P., and Raajenthirenen, M. (2008). "Fabrication and characterization of CA/PSf/SPEEK ternary blend ultrafiltration membranes," *Ind. Eng. Chem. Res.* 47(5), 1488-1494. DOI: 10.1021/ie070810k

Bai, H. L., Wang, X., Sun, H. B., and Zhang, L. P. (2015). "Permeability and morphology study of polysulfone composite membrane blended with nanocrystalline cellulose," *Desalin. Water Treat* 53, 11, 2882-2896. DOI: 10.1080/19443994.2013.875944

Chang, L. S., Su, T. L., Yang, M. C., and Kung, F. C. (2010). "Effect of diallyl disulfide immobilization on the immunoreaction of polysulfone membranes," *Text. Res. J.* 80(11), 1038-1046. DOI: 10.1177/0040517509352519

Chen, S. H., Yu, K. C., Lin, S. S., Lin, D. J., and Liou, R. M. (2001). "Pervaporation separation of water/ethanol mixture by sulfonated polysulfone membrane," *J. Membr. Sci.* 183(1), 29-36. DOI: 10.1016/S0376-7388(00)00544-5

Deimede, V., Labou, D., and Neophytides, S. G. (2014). "Polymer electrolyte membranes based on blends of sulfonated polysulfone and PEO-grafted polyethersulfone for low temperature water electrolysis," *J. Appl. Polym. Sci.* 131(4), 39922.1-39922.8. DOI: 10.1002/APP.39922

Geise, G. M., Lee, H. S., Miller, D. J., Freeman, B. D., Mcgrath, J. E., and Paul, D. R. (2010). "Water purification by membranes: The role of polymer science," *J. Polym. Sci. Pol. Phys.* 48(15), 1685-1718. DOI: 10.1002/polb.22037

Goetz, L., Mathew, A., Oksman, K., Gatenholm, P., and Ragauskas, A. J. (2009). "A novel nanocomposite film prepared from crosslinked cellulosic whiskers," *Carbohyd. Polym.* 75(1), 85-89. DOI: 10.1016/j.carbpol.2008.06.017

Gong, G. H., Wang, J. H., Nagasawa, H., Kanezashi, M., Yoshioka, T., and Tsuru, T. (2013). "Sol-gel spin coating process to fabricate a new type of uniform and thin organosilica coating on polysulfone film," *Mater. Lett*. 109, 130-133. DOI: 10.1016/j.matlet.2013.07.061

Jutemar, E. P., and Jannasch, P. (2010). "Influence of the polymer backbone structure on the properties of aromatic ionomers with pendant sulfobenzoyl side chains for use as proton-exchange membranes," *ACS Appl. Mater. Inter*. 2(12), 3718-3725. DOI: 10.1021/am1008612

Kumar, R., Isloor, A. M., Ismail, A. F., Rashid, S. A., and Matsuura, T. (2013a). "Polysulfone-chitosan blend ultrafiltration membranes: Preparation, characterization, permeation and antifouling properties," *RSC Adv*. 3(21), 7855-7861. DOI: 10.1039/c3ra00070b

Kumar, R., Isloor, A. M., Ismail, A. F., and Matsuura, T. (2013b). "Performance improvement of polysulfone ultrafiltration membrane using N-succinyl chitosan as additive," *Desalination* 318, 1-8. DOI: 10.1016/j.desal.2013.03.003

Li, R. J., Fei, J. M., Cai, Y. R., Li, Y. F., Feng, J. Q., and Yao, J. M. (2009). "Cellulose whiskers extracted from mulberry: A novel biomass production," *Carbohyd. Polym.* 76(1), 94-99. DOI: 10.1016/j.carbpol.2008.09.034

Li, S., Gao, Y., Bai, H. L., Zhang, L. P., Qu, P., and Bai, L. (2011). "Preparation and characteristics of polysulfone dialysis composite membranes modified with nanocrystalline cellulose," *BioResources* 6(2), 1670-1680. DOI: 10.15376/biores.6.2.1670-1680

Ma, Y. X., Shi, F. M., Ma, J., Wu, M. N., Zhang, J., and Gao, C. J. (2011). "Effect of PEG additive on the morphology and performance of polysulfone ultrafiltration membranes," *Desalination* 272(1-3), 51-58. DOI: 10.1016/j.desal.2010.12.054

Padaki, M., Isloor, A. M., Wanichapichart, P., and Ismail, A.F. (2012). "Preparation and characterization of sulfonated polysulfone and N-phthloyl chitosan blend composite cation-exchange membrane for desalination," *Desalination* 298, 42-48. DOI: 10.1016/j.desal.2012.04.025

Qu, P., Tang, H. W., Gao, Y., Zhang, L. P., and Wang, S. Q. (2010). "Polyethersulfone composite membrane blended with cellulose fibrils," *BioResources* 5(4), 2323-2336. DOI: 10.15376/biores.5.4.2323-2336

Rahimpour, A., and Madaeni, S. S. (2007). "Polyethersulfone (PES)/cellulose acetate phthalate (CAP) blend ultrafiltration membranes: Preparation, morphology, performance and antifouling properties," *J. Membr. Sci.* 305(1–2), 299-312. DOI: 10.1016/j.memsci.2007.08.030

Rahimpour, A., Madaeni, S. S., Ghorbani, S., Shockravi, A., and Mansourpanah, Y. (2010). "The influence of sulfonated polyethersulfone (SPES) on surface nano-morphology and performance of polyethersulfone (PES) membrane," *Appl. Surf. Sci.* 256(6), 1825-1831. DOI: 10.1016/j.apsusc.2009.10.014

Rosa, M. F., Medeiros, E. S., Malmonge, J. A., Gregorski, K. S., Wood, D. F., Mattoso, L. H. C., Glenn, G., Orts, W. J., and Imam, S. H. (2010). "Cellulose nanowhiskers from coconut husk fibers: Effect of preparation conditions on their thermal and morphological behavior," *Carbohyd. Polym.* 81(1), 83-92. DOI: 10.1016/j.carbpol.2010.01.059

Tang, Y. J., Xue, Z. G., Zhou, X. P., Xie, X. L., and Tang, C. Y. (2014). "Novel sulfonated polysulfone ion exchange membranes for ionic polymer-metal composite actuators," *Sensor. Actuat. B-Chem.* 202, 1164-1174. DOI: 10.1016/j.snb,2014.06.071

Tran, A. T. T., Patterson, D. A., and James, B. J. (2012). "Investigating the feasibility of using polysulfone-montmorillonite composite membranes for protein adsorption," *J. Food Eng.* 112(1–2), 38-49. DOI: 10.1016/j.jfoodeng.2012.03.031

Xin, Y. H., and Wang, S. Z. (1994). "An investigation of sulfonated polysulfone humidity-sensitive materials," *Sensor. Actuat. A-Phys.* 40(2), 147-149. DOI: 10.1016/0924-4247(94)85021-6

Zhao, S., Wang, Z., Wei, X., Tian, X. X., Wang, J. X., Yang, S. B., and Wang, S. C. (2011). "Comparison study of the effect of PVP and PANI nanofibers additives on membrane formation mechanism, structure and performance," *J. Membr. Sci.* 385(1–2), 110-122. DOI: 10.1016/j.memsci.2011.09.029

Zhao, X. T., Su, Y. L., Li, Y. F., Zhang, R. N., Zhao, J. J., and Jiang, Z. Y. (2014). "Engineering amphiphilic membrane surfaces based on PEO and PDMS segments for improved antifouling performances," *J. Membr. Sci.* 450, 111-123. DOI: 10.1016/j.memsci.2013.08.044

Zuluaga, R., Putaux, J. L., Cruz, J., Velez, J., Mondragon, I., and Ganan, P. (2009). "Cellulose microfibrils from banana rachis: Effect of alkaline treatments on structural and morphological features," *Carbohyd. Polym.* 76(1), 51-59. DOI: 10.1016/j.carbpol.2008.09.024